JOURNAL OF GUIDANCE, CONTROL, AND DYNAMICS
Vol. 15, No. 4, July-August 1992

High-Bandwidth Positioning Control of Small Payloads Mounted on a Flexible Structure

James G. Garcia,* Lisa A. Sievers,* and Andreas von Flotow†
Massachusetts Institute of Technology, Cambridge, Massachusetts 02139

This paper considers the problem of high-bandwidth positioning and pointing of a small mass mounted on a flexible structure. A potential application would be the positioning of mirrors in a space-based interferometer. For high-performance control it is a general rule that a sufficiently accurate model of the plant is needed in the control bandwidth, particularly at crossover. Determining a sufficiently accurate model of a flexible structure over a broad frequency band is a very difficult problem. This paper points out that, for small payloads, the plant transfer function from control actuation to sensing is only lightly perturbed from what it would be if the structure was rigid. The paper identifies a bound on the gain and phase perturbations of the plant as a function of the ratio of the payload mass to modal mass of the structure. It is shown that, when this ratio is small enough, a high-performance stable controller can be designed without further consideration of the structural dynamics. Experimental results are presented that quantitatively support the predictions.

Introduction

MANY flight systems require the pointing of an optical element at a target with high precision over a wide bandwidth. These devices typically use movable mirrors to track an object or to correct for high-frequency disturbances. If the mirror mass is light enough relative to the structural mass, or if the structure has sufficient damping, the mirror can be positioned with simple control without the risk of unstable interaction with structural dynamics. However, when the actuated mass is too large, the pointing performance or stability of the system may be affected as the flexible modes in the structure are excited. More complicated measures must be taken to address the problem, such as high-order controllers or mechanical redesign.

One class of actuated mass systems are flight optical communication packages that use small actuated mirrors to take out low-amplitude pointing errors at high frequency. These devices usually correct errors in two or more increasingly finer stages.[1] Other systems, such as aircraft- or space-based cameras, use gimbal-mounted tracking mirrors to steer incoming light from various angles onto a fixed optical train. Large, ground-based stellar interferometers and test beds of space-based interferometers use actuated mirrors to correct optical path length errors.[2,3] Reactionless mirrors can be used to effectively reduce the actuated mass. The simplest of these "reactuators" contains an additional mass, with an equal mass-stroke product as the mirror, which moves opposite to the mirror.

In this paper a relationship between the system parameters is defined that quantifies the effect of structural flexibility on the dynamics "seen" by the control system. The relevant dimensionless parameter group is formulated as

$$(m_m/\overline{m}_i)(1/\zeta_i) \tag{1}$$

where m_m is the mirror mass, $\overline{m}_i$ the effective modal mass at the mirror mounting location, and ζ_i the modal damping ratio. This paper demonstrates that this group governs the degree to which flexibility participates in the dynamics and shows that flexibility can be ignored if this group is much less than unity. The concepts are then demonstrated experimentally.

Figure 1 shows two mirrors located at different locations on a flexible structure. This paper is concerned with the high-bandwidth control of the inertial position y_2 and also with the relative position of the two mirrors, $y_2 - y_3$. When y_2 is the variable to be controlled, the sensor actuator pair is termed collocated; i.e., the sensor is at the same location as the actuator. The other configuration, when $y_2 - y_3$ are to be controlled, is termed noncollocated; i.e., relative displacement is sensed, but actuation occurs only at y_2.

Theory

System Configuration

To simplify this discussion, a single-axis translation of the actuated mirror is modeled. An obvious change of notation makes the analysis directly applicable to pointing with rotation of the actuated mirror about its mass center. The theory

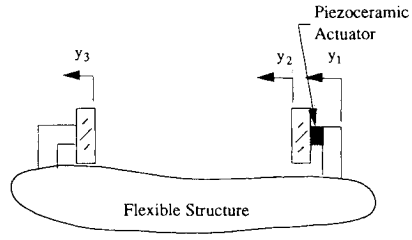

Fig. 1 Fixed and actuated mirrors on a flexible structure.

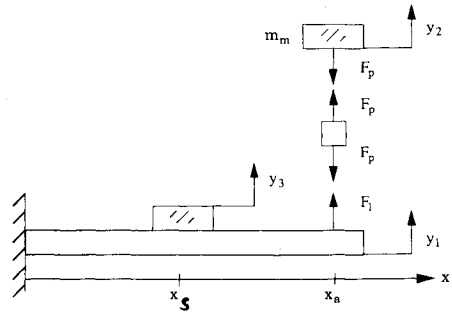

Fig. 2 Free-body diagram of actuated mirror on beam.

Received Sept. 18, 1991; revision received Nov. 18, 1991; accepted for publication Dec. 17, 1991. Copyright © 1992 by the American Institute of Aeronautics and Astronautics, Inc. All rights reserved.

*Research Assistant, Department of Aeronautics and Astronautics.
†Associate Professor, Department of Aeronautics and Astronautics.

is applicable to multiple-axis interaction with appropriate, although possibly complex, generalizations.

The system shown in Fig. 2 is a free-ended cantilever beam with an actuated plane mirror mounted at the tip and a secondary mirror mounted somewhere along the beam. The mirror positions, y_2 and y_3, are measured by an externally located laser measurement system as that shown in Fig. 3. The collocated control objective is to regulate y_2. The noncollocated control objective is to regulate the difference, $y_3 - y_2$, by employing the actuator at y_2.

This section develops a model relevant to any linear flexible structure, but uses terminology specific to the beam of Fig. 2. Using standard structural dynamic modeling techniques, the transfer function between a deflection and an applied force is

$$\frac{y_1(s)}{F_1(s)} = \sum_{i=1}^{\infty} \frac{\alpha_i \beta_i}{m_i(s^2 + 2\zeta_i \omega_i s + \omega_i^2)} \tag{2}$$

The variables α_i and β_i depend on the force and sensing details, and m_i is the modal mass of the structure. If the force is taken to be a point force, F_1, applied by the actuator at a point $x = L$ along the length of the beam, then $\alpha_i = \Phi_i(L)$. Similarly, if the sensor measures displacement at a point $x = L$, then $\beta_i = \Phi_i(L)$. The function $\Phi_i(x)$ is the ith natural mode of vibration of the structure without the actuated mirror. If the mount is at the tip of the depicted beam, $\Phi_i(L) = \pm 2$ since the mode shapes are normalized so that the tip deflection is 2 (Ref. 4). At this point it is useful to define the "effective" modal mass, $\overline{m}_i = m_i/\alpha_i\beta_i$, also identifiable as the inverse of the modal residue. This quantity is defined as

$$\overline{m}_i = \frac{\int_0^L \Phi_i^2(x)dm}{\alpha_i \beta_i} \tag{3}$$

and is independent of mode shape normalization. For a uniform beam with the normalization mentioned earlier, the absolute value of the denominator term, $\alpha_i\beta_i$ can vary from a minimum of zero, when either the sensor or the actuator is located on a node, to 4, when they are both on the beam tip. When the sensor and the actuator are located on antinodes, the minimum effective modal mass will equal one-half the mass of the beam for mode shapes sinusoidal in space. When the actuator is located on a node, the effective modal mass is infinite, since the actuating force has no effect on the beam motion. When the sensor is located on a node, the effective modal mass is also infinite, since the sensor location is not affected by the motion caused by the actuator. The former example results in an uncontrollable mode, whereas the latter results in an unobservable mode. If the sensor and actuator are not collocated, the effective modal mass can be negative.

A piezoceramic block is the actuator used in the example central to this paper. Piezoceramic actuators are ceramic devices that produce an electric charge when stressed mechanically and strain mechanically when an electric field is applied.

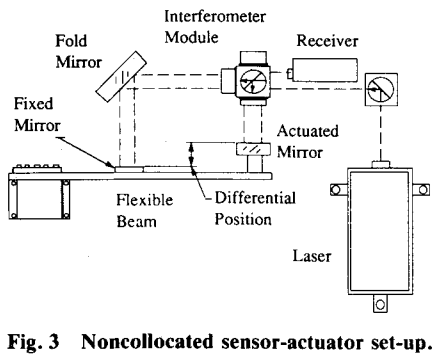

Fig. 3 Noncollocated sensor-actuator set-up.

As the actuator is driven by a voltage across its terminals, the actuated mirror's mass is reacted by the beam as shown in Fig. 2. The piezoceramic can be described by

$$F_p = k(y_2 - y_1 - dV) = F_1 \tag{4}$$

$$F_p = -m_m s^2 y_2 \tag{5}$$

where k is the stiffness of the piezoceramic actuator, V is the voltage, d is the displacement to voltage constant for the actuator, and m_m is the effective mirror mass. Note that the mass of the piezoceramic is ignored or lumped partially with the mirror mass and partially with the beam, as appropriate.

The rest of this paper will continue with this model of the actuator, but many of the conclusions are valid for other actuator models. If the actuator is assumed to be a perfect force actuator, then clearly the collocated plant transfer function, $y_2/F_p = -1/m_m s^2$, is independent of the structural dynamics. However, the noncollocated plant transfer function $(y_2 - y_3)/F_p$ will reflect the structural dynamics in a way that is quantified in the appropriate sections of this paper. Other actuator models require a bit more thought; one way to think about actuators is in terms of their output impedance (i.e., zero for a perfect force actuator and infinite for a perfect stroke actuator).

Plant Transfer Function for Collocated Sensor and Actuator

We assume that the beam responds to reaction force F_1 according to

$$y_1 = H_1 F_1 \tag{6}$$

where H_1 is the driving point compliance of the beam:

$$H_1 = \frac{y_1}{F_1} = \sum_{i=1}^{\infty} \frac{1}{\overline{m}_i(s^2 + 2\zeta_i \omega_i s + \omega_i^2)} \tag{7}$$

The component models, Eqs. (4-6) may now be assembled into a plant transfer function of the sensor output to the control input:

$$\frac{y_2}{dV} = \frac{1}{\left(1 + \dfrac{m_m s^2}{k} + m_m s^2 H_1\right)} \tag{8}$$

The term in the denominator, $m_m s^2/k$, is very small compared to unity and can be neglected without loss of accuracy for frequencies less than the natural frequency of the mirror/actuator subsystem (7 kHz in the experiment). Therefore,

$$\frac{y_2}{dV} = \frac{1}{1 + m_m s^2 H_1} \tag{9}$$

It should be apparent from Eqs. (7) and (9) that the poles of the driving point compliance of the beam (H_1) become the zeros of the plant transfer function (y_2/dV). Therefore, the zeros of Eq. (9) are approximately at $\overline{z}_1 = \omega_i(-\zeta_i \pm j)$.

Pole-Zero Spacing of the Collocated Plant Transfer Function

Undamped flexible structures with collocated sensor-actuator pairs have a useful property that makes the system easier to control. The poles and zeros of the driving point compliance, $H_1(s)$, alternate along the imaginary axis of the complex plane, keeping the phase within a 180-deg range. Figure 4 shows a typical pattern of poles and zeros in the complex plane, here arbitrarily assumed to be uniform modal damping. The arguments we develop do not depend on details of the damping model, but assume only that the damping is light.

Using only this property of the point compliance, Sievers and von Flotow[5] show algebraically that the undamped plant

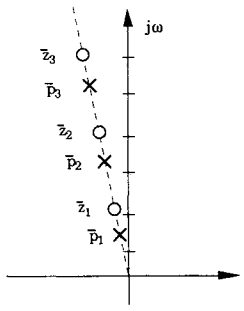

Fig. 4 Poles and zeros of the point compliance H_1 in the complex plane.

transfer function [Eq. (9)] also has alternating poles and zeros along the $j\omega$ axis. Thus, the plant transfer function for the collocated case also has the useful property of a phase that varies between 0 and -180 deg.

Although the location of the plant zeros is clear from Eq. (9) (they are the poles of H_1), the pole locations are not as obvious, unless, of course, the mirror mass is zero. For this limiting case the poles overlap the zeros and the flexibility is irrelevant to the plant dynamics. It might be conjectured that, as the mass of the mirror increases, the poles start to move away from the zeros. In fact, for a small mirror mass it is possible to determine a maximum pole-zero spacing using root locus ideas, with actuated mass m_m acting as the root locus gain.

If it is assumed that there is no damping, and the structural eigenfrequencies (the poles of H_1) are sufficiently widely spaced, then it can be shown[6] that the plant pole, $\bar{p}_i = j\omega_{\bar{p}_i}$, occurs at a frequency somewhat below the plant zero $\bar{z}_i = j\omega_i$. In fact, the pole location is bounded by the following inequalities:

$$\omega_i \geq \omega_{\bar{p}_i} > \frac{1}{\sqrt{1 + (m_m/\bar{m}_i)}}\,\omega_i \tag{10}$$

The pole-zero spacing along the complex axis for the ith mode is thus (to first order in $m_m/\bar{m}_i$):

$$\omega_i - \omega_{\bar{p}_i} \leq \tfrac{1}{2}(m_m/\bar{m}_i)\,\omega_i \tag{11}$$

This expression becomes an equality if this predicted pole-zero spacing is not so large that the plant pole $\bar{p}_i$ approaches the next lower plant zero, $\bar{z}_{i-1}$.

These results can be derived assuming a plant with no damping. The pole-zero pattern of a lightly damped structure differs from that of an undamped structure only in the real part of the corresponding roots. A first-order perturbation argument[7] shows that the imaginary part is unchanged. Therefore, the pole-zero frequency spacing of Eq. (11) is assumed correct for lightly damped structures.

The plant transfer function of Eq. (9) can now be written in a simpler form, which highlights pole-zero near cancellation:

$$\left(\frac{y_2}{dV}\right)_i = \frac{\prod_{i=-\infty}^{\infty}[1-(s/\bar{z}_i)]}{\prod_{i=-\infty}^{\infty}[1-(s/\bar{p}_i)]}; \quad \text{where} \quad \bar{z}_i = \omega_i(-\zeta_i \pm j), \quad \bar{p}_i \cong \bar{z}_i\left(1 - \frac{1}{2}\frac{m_m}{\bar{m}_i}\right) \tag{12}$$

The inequality bound of Eq. (11) becomes an equality in the limit as the modal spacing of the flexible structure becomes large compared to the pole-zero spacing. In this limit the plant transfer function in the frequency band about the ith pole can be simplified to a single second-order pole-zero pair that is not affected by adjacent modes:

$$\frac{y_2}{dV} \cong \frac{s^2 + 2\zeta_i\omega_i s + \omega_i^2}{[1 + (m_m/\bar{m}_i)]s^2 + 2\zeta_i\omega_i s + \omega_i^2} \tag{13}$$

Gain and Phase Due to Flexibility

The preceding section has demonstrated that each flexible mode of the substructure contributes a pole-zero pair to the plant transfer function. A simple bound on the gain and phase contributions of each of the pole-zero pairs can be found if it is assumed that the modal overlap of the flexible structure is low. By use of geometric or algebraic arguments, it is easy to show that the maximum phase contribution of the pole-zero pair $(\bar{p}_i, \bar{z}_i)$ corresponding to the ith mode is (to first order in $m_m/\bar{m}_i$)

$$\text{Phase} \cong -2\tan^{-1}\left(\frac{1}{4\zeta_i}\frac{m_m}{\bar{m}_i}\right) \tag{14}$$

and occurs at a frequency midway between $\omega_{\bar{p}_i}$ and ω_i. Outside the interval $(\bar{p}_i, \bar{z}_i)$, this pole-zero pair contributes negligible phase. The maximum phase for structures with higher modal overlap can also be derived.[6] For this case the maximum phase of Eq. (14) has additional terms due to the phase contributions of neighboring pole-zero pairs.

For the case of low modal overlap the gain effects of the pole-zero pair $(\bar{p}_i, \bar{z}_i)$ are also limited to the immediate frequency vicinity. A maximum gain excursion occurs at the natural frequency of each of the poles. Therefore, a maximum in gain can be calculated from Eq. (13) and is approximately equal to

$$\text{Gain} \cong \sqrt{\{1 + [(1/2\zeta_i)(m_m/\bar{m}_i)]^2\}} \tag{15}$$

Both the phase excursions [Eq. (14)] and the gain excursion [Eq. (15)] depend on the ratio $m_m/(\zeta_i\bar{m}_i)$. High damping is thus comparable to light mirrors in mitigating the effect of structural flexibility. The dimensionless group that governs the degree of interaction of the control system with the flexibility is clearly $m_m/(\zeta_i\bar{m}_i)$.

Extension to the Noncollocated Case

When the sensor and actuator are not positioned at the same point, the control problem generally becomes much more difficult because of the structural flexibility between the two points. However, if the actuated mass is light enough, the system should still be simple; in the limit of massless mirrors the structural flexibility will not appear in the plant transfer function. In this section the characteristics of the system as a function of the ratio of actuated mass to modal mass and of damping will again be determined, but for a noncollocated sensor and actuator pair.

The variables used to describe the model parameters for the noncollocated case are specific to the beam of Fig. 2. The noncollocated plant transfer function is

$$\frac{y_2 - y_3}{dV} = \frac{(1 + H_3 m_m s^2)}{[1 + (m_m s^2/k) + H_1 m_m s^2]} \tag{16}$$

where H_1 is the collocated driving point compliance of the beam [Eq. (7)]:

$$H_1 = \sum_{i=1}^{\infty} \frac{1}{\bar{m}_i(s^2 + 2\zeta_i\omega_i s + \omega_i^2)} \tag{17a}$$

and where

$$\overline{m}_i = \frac{\int_0^L \Phi_i^2(x)dm}{\Phi_i^2(L)} \tag{17b}$$

and H_3 is the noncollocated compliance of the beam:

$$H_3 = \sum_{i=1}^{\infty} \frac{1}{\hat{m}_i(s^2 + 2\zeta_i\omega_i s + \omega_i^2)} \tag{18a}$$

where

$$\hat{m}_i = \frac{\int_0^L \Phi_i^2(x)dm}{\Phi_i(L)\Phi_i(x_s)} \tag{18b}$$

Equation (16) can be simplified, as in the collocated case, if it is assumed that only low frequencies are of interest, i.e., where $m_m s^2 << k$.

The noncollocated plant transfer function can be viewed as a product of two simpler transfer functions, one of which is identical to the collocated plant transfer function of Eq. (9):

$$\frac{y_2 - y_3}{dV} = \left[\frac{1}{1 + m_m s^2 H_1}\right]\left[\frac{1}{1 + m_m s^2 H_3}\right]^{-1} \tag{19}$$

$$\frac{y_2 - y_3}{dV} = \left[\frac{\prod_{i=-\infty}^{\infty}(1 - s/\overline{z}_i)}{\prod_{i=-\infty}^{\infty}(1 - s/\overline{p}_i)}\right]\left[\frac{\prod_{i=-\infty}^{\infty}(1 - s/\hat{z}_i)}{\prod_{i=-\infty}^{\infty}(1 - s/\hat{p}_i)}\right]^{-1}$$

$$= \left[\frac{\prod_{i=-\infty}^{\infty}(1 - s/\hat{p}_i)}{\prod_{i=-\infty}^{\infty}(1 - s/\overline{p}_i)}\right] \tag{20}$$

The poles and zeros of the second bracketed term of Eq. (19) are labeled $\hat{p}_i$ and $\hat{z}_i$, respectively. It should be apparent that the poles of the beam driving point compliance are the zeros in Eq. (20); thus $\overline{z}_1 = \hat{z}_i = \omega_i(-\xi_i \pm j)$.

The bounds on the roots of the collocated open-loop plant $\overline{p}_i$, are already known from the prior discussion. A similar argument yields values for $\hat{p}_i$, in Eq. (20), where the mirror mass can be viewed as the root locus "gain" as before. This time, however, the effective noncollocated modal mass $\hat{m}_i$ may be negative, which corresponds to a structural mode in which the product $\Phi(L)\Phi(x_s)$ is negative. In this case, $|\hat{p}_i| > |\overline{z}_i|$. The roots, $\hat{p}_i$, become zeros of the plant transfer function, as is clear from Eq. (20). The plant zero thus stays close to the structural eigenfrequency, ω_i, as does the plant pole. The bound on the zero motion is determined from the noncollocated effective modal mass, and the bound on the pole motion is determined from the collocated effective modal mass. The pole-zero spacing for the plant will thus be a function of the collocated effective modal mass and the noncollocated effective modal mass.

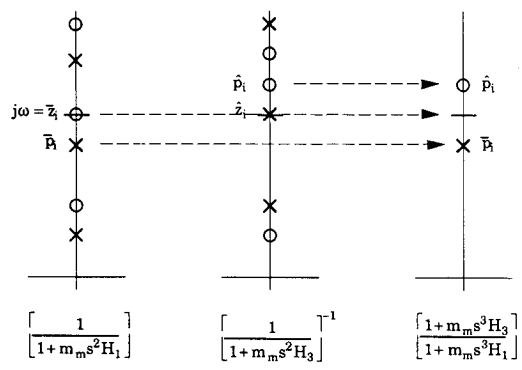

Fig. 5 Worst case pole-zero spacing for the noncollocated plant.

Figure 5 summarizes the discussion graphically. The plant transfer function [Eq. (21)] has a sequence of pole-zero pairs along the $j\omega$ axis. The ordering of the pole and zero in each pair depends on the relative magnitude of $\overline{m}_i$ and $\hat{m}_i$, the effective modal masses. If $\overline{m}_i$ and $\hat{m}_i$ are of opposite sign, then the pole-zero spacing will be greatest, the pole $\overline{p}_i$ will be at a lower frequency than the zero $\hat{p}_i$, and the spacing will be (exact to first order in $m_m/\overline{m}_i$ and $m_m/\hat{m}_i$)

$$|\hat{p}_i| - |\overline{p}_i| \cong \frac{1}{2}\left(\frac{m_m}{\overline{m}_i} - \frac{m_m}{\hat{m}_i}\right)\omega_i \tag{21}$$

If the noncollocated effective modal mass is positive, the plant zero $\hat{p}_i$ will move downward toward the plant pole $\overline{p}_i$, giving a smaller pole-zero spacing. In the limit of small mirror mass and sufficient modal spacing, the plant transfer function in a frequency band about the ith pole-zero pair can be simplified to a single pole-zero pair that is not affected by adjacent modes:

$$\frac{y_2 - y_3}{dV} \cong \frac{(1 + m_m/\hat{m}_i)s^2 + 2\zeta_i\omega_i s + \omega_i^2}{(1 + m_m/\overline{m}_i)s^2 + 2\zeta_i\omega_i s + \omega_i^2} \tag{22}$$

The foregoing development was specific to piezoceramic actuation, but can be easily applied to other actuation techniques. For example, if one models the actuator as a perfect force actuator, the plant transfer will not depend on the collocated effective modal mass $\overline{m}_i$, but will display pole-zero pairs with spacing dependent only on $m_m/\hat{m}_i$.

Gain and Phase of the Noncollocated Plant Due to Flexibility

For a structure with low modal overlap the local minimum in phase is approximately halfway between the pole and zero, i.e., at $s = j[1 - m_m/(4\overline{m}_i) - m_m/(4\hat{m}_i)]\omega_i$.

The phase contributed in the noncollocated case by the ith mode is again limited by damping and by pole-zero spacing. Flexibility can introduce local phase lead, as should be obvious from Fig. 5. This occurs if $\Phi_i(x_s) > \Phi_i(L)$, i.e., if the secondary mirror location is driven more strongly than the actuator location by the actuation force. The maximum phase due to the ith mode is, to first order in $m_m/\overline{m}_i$ and $m_m/\hat{m}_i$,

$$\text{Phase} \cong -2\tan^{-1}\left[\frac{1}{4\zeta_i}\left(\frac{m_m}{\overline{m}_i} - \frac{m_m}{\hat{m}_i}\right)\right] \tag{23}$$

For structures with low modal overlap the maximum in the gain occurs at the plant pole $\overline{p}_i$. Therefore, the maximum in gain can be calculated from Eq. (22) and is approximated by the following expression:

$$\text{Gain} \cong \sqrt{\left\{1 + \frac{1}{4\zeta_i^2}\left[\frac{m_m}{\overline{m}_i} - \frac{m_m}{\hat{m}_i}\right]^2\right\}} \tag{24}$$

As in the collocated case, high damping is comparable to light mirrors in diminishing the effect of flexibility on the plant transfer function. The dimensionless groups that govern the degree of interaction of the control system with the flexibility are clearly $m_m/\zeta_i\overline{m}_i$ and $m_m/\zeta_i\hat{m}_i$.

Summary of Effect of Flexibility

The preceding subsections have presented the result that the plant transfer function (from the actuator command to the

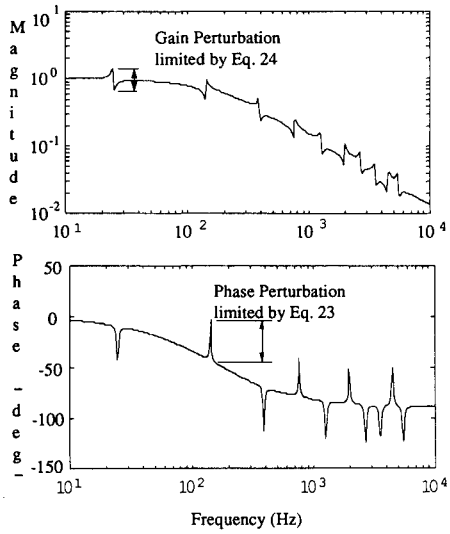

Fig. 6 Simulated plant transfer function, $(y_2 - y_3)/dV$.

absolute position of a mirror and also relative displacement of two mirrors) is that of a rigid plant with perturbations due to flexibility. Figure 6 is a simulation of these characteristics, along with the first-order rolloff of an amplifier. Note that some of the pole-zero pairs introduce local lead.

Experimental Validation of Bounds on Gain and Phase

Hardware Description

The collocated and noncollocated experiments were performed on an optical table. Two different beams were used for testing. The beams were mounted in a clamped-free configuration as shown in Fig. 3. The physical properties of each of the beams are listed in Table 1. The displacement of the mirror was monitored via a laser measurement system with a resolution of 2.2 nm.

A piezoceramic device was used for the actuator. The piezoceramic actuator had a displacement to voltage constant of 0.090 μ/V and a stiffness of 290 N/μ. The piezo was bonded to the aluminum plate using Scotchweld 2216 Gray two-part epoxy. The bondline thickness was maintained at 0.13 mm by use of a wire placed between the parts. The positive terminal of the piezo stack was routed through a 5-Ω, 5-W resistor to increase the reactance of the piezoactuator as seen by the voltage amplifier in case the piezo shorted out. This resistor combined with the capacitance of the piezo caused a substantial phase lag, which is discussed further in the following section.

The actuated mass was varied by adding weights to the mirror mount. The effective modal mass was varied by placing the fixed or actuated mirror at different locations on the beam. The damping was varied by adding a viscoelastic constraining layer to the beam.

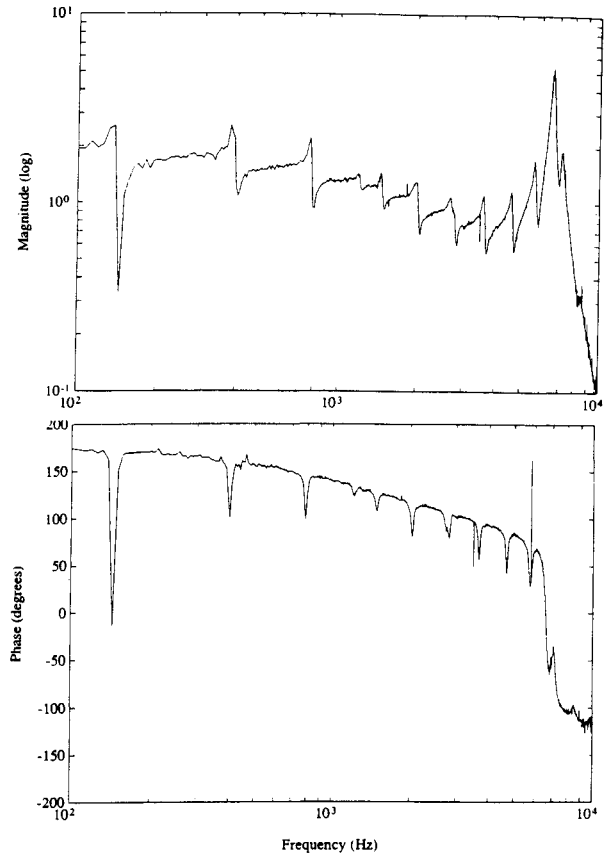

Fig. 7 Measured collocated plant transfer function of mirror at tip of flexible beam.

Experimental Results

Bounds on the phase and gain of the plant transfer function for the collocated and noncollocated configurations were derived analytically in the previous section. These bounds were listed in Eqs. (14) and (15) for the collocated case and Eqs. (23) and (24) for the noncollocated case. The goal of this experiment was to validate these bounds through comparison of experimental measurements with numerical predictions.

Plant transfer functions were measured using the beams described in Table 1 for both the collocated and noncollocated configurations. Figure 7 is an example of a measured collo-

Table 1 Physical properties of experimental beams

Beam no.	Material	Dimensions, in.	Damping
1	Steel	22 × 2 × 3/8	Single constrained layer
2	Aluminum	22 × 2 × 5/16	Double constrained layer

Table 2 Comparison of predicted and measured phase and gain bounds

Mode/ eigen-frequency	Measured ζ_i	Fixed mirror location	Calculated $\overline{m}_i$	Calculated $\hat{m}_i$	Predicted phase excursion, deg	Measured phase excursion, deg	Predicted gain excursion, dB	Measured gain excursion, dB
3/400	0.012	0.68	1.238	−1.750	−112	−105	—	—
3/400	0.012	0.64	1.238	−1.750	−100	−95	—	—
3/400	0.012	Coll.[a]	1.643	N/A	−80	−87	—	—
4/760	0.013	Coll.[a]	1.238	N/A	−78	−70	—	—
4/760	0.013	0.27	1.238	−1.750	−108	−112	—	—
6/2000	0.020	0.50	1.238	−1.750	−84	−75	—	—
7/2800	0.013	Coll.[a]	1.238	N/A	−78	−50	15.3	29.3
7/2800	0.013	0.27	1.238	−1.750	−108	−72	—	—
8/3600	0.01	Coll.[a]	1.238	N/A	−93	−78	—	

[a]Coll., collocated sensor and actuator at beam tip.

cated transfer function, as opposed to the simulated transfer function shown in Fig. 6. Since this is a collocated plant, all of the phase perturbations are negative. Notice, however, the low-pass filtering behavior due to the 5-Ω resistor in series with the piezoceramic capacitance and a sudden phase rolloff of 180 deg at 7000 Hz due to the eigenmode of the mirror and piezoactuator combination. This eigenmode was the resonant frequency of the mirror on the piezoactuator. This is where the assumption breaks down that $m_m s^2 << k$. Note that the phase starts at 180 deg because a positive mirror displacement is read as a shortening of the distance between the mirror and receiver.

To test the theoretical predictions, a comparison between the predicted and measured phase and gain excursions [Eqs. (23) and (24)] was attempted near the resonant frequencies. Table 2 presents the results of this comparison. The predicted phase was synthesized from estimates of damping ratio and effective modal mass. Unfortunately, these predictions use quantities that are only approximately known: modal damping ratio and effective modal mass. Of these, the damping ratio is perhaps the most difficult to quantify accurately.

The value of the damping ratios for the beam was determined using two different methods: a logarithmic decrement after a long, steady sinusoidal excitation at resonant frequency and a recursive lattice least-squares algorithm, performed on a Tektronix 2630 system analyzer.[8] The consistency of the results of this "canned" algorithm depended on the cleanliness of the transfer function data. The typical method used was burst random excitation while zooming in on the mode of interest. Unfortunately, the routine returned damping values that varied up to 30%, depending on the quantity of roots that the routine looked for. The most consistent results were achieved using a search criteria of about twice as many modes as were expected. The damping values also varied by 20% from different sets of measurement data, given the same test parameters and modal search criteria.

Estimates for effective modal mass and modal damping ratio were generated and used to predict gain and phase excursions. Table 2 shows reasonable agreement between the predicted phase bound and the experimental phase of the plant at each of the eigenfrequencies. Gain excursions were usually not recorded.

Implication for Control

Discussion

Implicit in the preceding development has been the tacit assumption that control of lightly damped structural dynamics is something that is best avoided. The approach taken in this work is to treat the structural dynamics as unstructured uncertainty and to use the preceding analysis to bound the phase and gain contribution. From the phase and gain perturbations one can predict the phase and gain margins and thus the stability of the loop. Broadband control is then possible, since one can then use simple control, e.g., position feedback with some type of rolloff, and leave sufficient gain and phase margins for the interaction with flexibility. For the system under consideration the equations developed give explicit expressions for the phase and gain margins required to maintain stability in the presence of flexibility. Perhaps more importantly, these equations also suggest techniques by which the impact of flexibility can be ameliorated:

1) reduction of actuated mass, perhaps by reaction against a local reaction mass rather than the structure;

2) increasing the effective modal mass by mounting the mirror near nodes of the substructure, or by increasing the mass of the substructure; and

3) increasing the passive damping of the structure.

The approach advocated is thus to base control on a low-order model that reproduces the gain and phase trends of the plant and to treat the contribution of the structural dynamics as bounded uncertainties. The more one knows about the flexibility, the more one will be able to depart from this simple approach and dynamically compensate the flexible dynamics. This would be done selectively, mode by mode, not necessarily in order of modal eigenfrequency, but rather near crossover or for strongly interacting modes.

Experimental Demonstration

The performance that can be achieved with simple proportional control is described. The purpose of the compensator was to command the actuated mirror to track out any motion as sensed by the laser measurement system. Since most of the disturbancies are at low frequencies and since high-frequency noise in the loop creates problems at high frequencies, a single-order rolloff was added to the position feedback controller. The loop transfer function was thus constant at low frequencies (the piezoceramic gave a stroke proportional to the commanded voltage) and incorporated second-order rolloff, a first-order pole at 4500 Hz due to the resistor in series with the piezoceramic, and a first-order pole of variable frequency (normally at 150 Hz) in the feedback loop.

By moving the secondary mirror to selected locations along the beam, and by selecting the compensator corner frequency and gain, any mode could be chosen to interact unstably with the control system. Moving the sensor mirror to a different location along the beam modified the plant transfer function by changing the degree to which different flexible modes contributed; the modes with antinodes near the sensing mirror contributed strongly, whereas those with nodes near the sensing mirror contributed weakly. Moving the compensator corner frequency affected the entire phase trend and, consequently, affected the phase and gain margins of each mode. Thus, any mode could be selectively driven unstable.

In the collocated case all that can be varied is the compensator corner frequency and the actuated mass. By reducing the corner frequency and increasing the gain, a sequence of modes can be destabilized in rough inverse order of eigenfrequency. Alternatively, increasing the mirror mass, given a collocated configuration, destabilized lower- and lower-frequency modes at ever lower values of gain.

Achievable Performance

To prevent this discussion of instability from suggesting that a reasonable performance in disturbance rejection is not achievable, performance achieved with the laboratory setup is presented here. Unfortunately, since no independent sensor was available for performance evaluation, it was difficult to separate the rejection of mechanical disturbances acting on the beam (acoustic, seismic, and air currents) from the rejection of sensor noise (electrical noise and atmospheric perturbations in the optical path). It is suspected that much of the achieved improvement in the sensed signal was actually the result of the mirror moving in order to track out sensor noise.

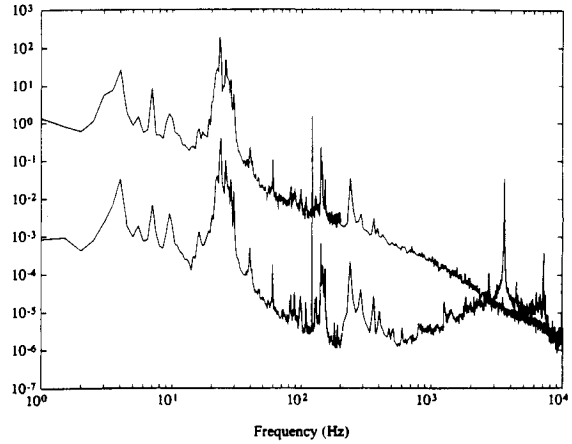

Fig. 8 Open- and closed-loop spectral density of mirror displacement, 0–20,000 Hz, beam 1, (m_m/m_b = 0.006).

The performance criteria experimentally measured were the rms and the peak-to-peak amplitude of the mirror. The performance results showed that the mirror motion could be controlled to fairly low amplitudes. The peak motion was generally around 250 nm peak to peak for the steel beam and 350 nm for the aluminum beam when excited by ambient laboratory disturbances. When the loop was closed, the low-frequency motion was markedly reduced—usually down to ~20 nm peak to peak.

Figure 8 shows a typical autospectrum of the rms mirror displacement for both controlled and uncontrolled cases for a collocated sensor and actuator. The controller used was a position feedback with a single pole rolloff at 150 Hz. As the gain was increased, the low-frequency disturbances were tracked out very well, but the noise and disturbances were amplified at the higher modes, eventually driving one of them unstable.

Summary

This paper has theoretically and experimentally quantified the importance of structural flexibility in the active control of positioning of a single small payload that was either absolute, with respect to an external reference, or relative, with respect to another part of the flexible structure. It has been demonstrated that the dimensionless group that governs the flexibility in the control problem is $m_m/(m_i \zeta_i)$, which can be evaluated on a mode-by-mode basis. Algebraic expressions were derived for the maximum gain and phase contributions to be expected from each mode as a function of this parameter, and the practical difficulties in estimating the parameter accurately were discussed. It was also shown both analytically and experimentally that, when this ratio is small enough, a stable controller can be designed without further consideration of the structural dynamics.

References

[1]Chan, V. W. S., "Laser Intersatellite Communication Systems," *Lincoln Laboratory Journal,* Vol. 2, 1989.

[2]Laskin, R. A., and San Martin, M., "Control/Structure System Design of a Spaceborne Optical Interferometer," AAS/AIAA Astrodynamics Specialist Conference, Stowe, VT, Aug. 7–10, 1989.

[3]Kissel, G., "Siderostat and Fast Steering Mirror Compensator Designs," Jet Propulsion Lab. Engineering Memo 343-1158, Sept. 1989.

[4]Blevins, R. D., *Formulas for Natural Frequency and Mode Shape,* Krieger, Malabar, FL, 1984.

[5]Sievers, L., and von Flotow, A., "Active Vibration Isolation in the Presence of Unmodeled Structural Dynamic Response," Proceedings of ASME, WAM, San Francisco, CA, Dec. 1989.

[6]Garcia, J. G., "Stability of Actuated Mirror on a Flexible Structure as a Function of Mass and Structural Damping," SM Thesis, Massachusetts Institute of Technology, Cambridge, MA, June 1990.

[7]Plaut, R. H., and Huseyin, K., "Derivatives of Eigenvalues and Eigenvectors in Non-Self Adjoint Systems," *AIAA Journal,* Vol. 11, No. 2, Feb. 1973, pp. 250–251.

[8]*Tektronix 2630 Personal Fourier Analyzer Operation Manual,* Tektronix, Inc., Campbell, CA, Sept. 1989.